Numerical Weather Prediction

Satellite Application Facility

SAF Programme

Research Report No. 3

Model clouds as seen from space: comparison with geostationary imagery in the 11μm window channel

by

Frédéric Chevallier and Graeme Kelly

Accepted for publication in Mon. Wea. Rev.

July 2001

Abstract

A monitoring of the European Centre for Medium-Range Weather Forecasts (ECMWF) model with the Meteosat infrared window channel during December 2000 is presented. The Meteosat images are simulated every three hours during the 31 days from the model fields, at a resolution of 35 *km*. The study of both the spatial and the temporal variabilities of the model cloudiness is based on forecasts, from 3 to 48 hours, as well as on analyses. Despite a reduced cloud forcing in the model, the variations of the extra-tropical cyclones are shown to be well represented in the short range (up to one day) forecasts. The Inter-Tropical Convergence Zone (ITCZ) is well located but the representation of its temporal variations significantly differs from the observations, in particular over land. The variability of the Meteosat brightness temperature time series usually differs by more than 10% from one model grid point to another, whereas the structures described by the model have scales of about three to four grid points at least.

This work prepares the routine monitoring of the ECMWF analysis and forecast system with the raw images from Meteosat, soon to be replaced by the Meteosat Second Generation imager/sounder, and is an important step towards the assimilation of cloud-affected satellite radiances.

1 Introduction

Operational geostationary satellites provide high-resolution (a few kilometres) and frequent (one hour or less) observations of the visible and infrared radiation that is emitted or reflected by a large portion of the Earth-atmosphere system. In forecast centres, geostationary imagery is essential for now-casting. Atmospheric motion winds derived from these data are routinely assimilated (Velden *et al.* 1992; Schmetz *et al.* 1993; Rohn *et al.* 2001) and the assimilation of clear-sky raw radiances will be operational in the near future (Munro *et al.* 2000). The validation of Numerical Weather Prediction (NWP) systems also makes use of derived cloud products (Rossow and Schiffer 1983; Jakob 1999) and of raw radiances (Morcrette 1991; Yu *et al.* 1997) It has been emphasised in previous studies that for validation as well as for assimilation, derived products may be ambiguous because they are to be understood as *radiatively effective* quantities, in the sense that they are defined as seen from the satellite (Velden *et al.* 1997; Chevallier *et al.* 2001), and as such they are pre-processed products with questionable errors associated to this processing. Therefore, effort is made to develop the use of raw radiances.

The high spatial resolution of the geostationary images makes it necessary to perform some averaging when comparing to model data. The resolution of global models has been dramatically increased over the last years so that synoptic scales are better taken into account. As an example, in late autumn 2000 the horizontal resolution of the European Centre for Medium-Range Weather Forecasts (ECMWF) operational forecasting system was increased from a T_L319 spectral representation (about 60 *km* resolution) to a T_L511 one (about 40 *km* resolution) on a global scale. Test versions are being run at T_L799 (about 25 *km* resolution).

In this paper, infrared window ($11\mu m$) images from the two Meteosat satellites operated by the European organization for the Exploitation of Meteorological Satellites (EUMETSAT) are compared to the simulated images from the ECMWF system. The comparison focuses on the month of December 2000: the Meteosat images are simulated every three hours. The data and the model are described in section 2. The Meteosat images allow the investigation of both the

Observation time (UTC)	03:00	06:00	09:00	12:00	15:00	18:00	21:00	24:00
Forecast range (hours)	3	6	9	12	3	6	9	12

Table 1: Forecast ranges used here for the simulation of the Meteosat images during December 2000.

spatial and the temporal variabilities of the cloudiness in the ECMWF analyses and forecasts. The results are presented in section 3 and are discussed in section 4.

2 The data

2.1 The Meteosat observations

Two Meteosat satellites were operational during December 2000. Meteosat-7 was positioned at the longitude and latitude origin, Meteosat-5 was located above the Indian ocean, at longitude 63°E on the Equator. Their on-board radiometers measure radiation from the Earth disc every 30 minutes in three spectral bands: the visible from 0.45 to 1.0 μm, the infrared 5.7-7.1 μm water vapour absorption band and the infrared window 10.5-12.5 μm band. This study makes use of the data from the infrared window channel, which is mainly sensitive to the vertical distribution of cloud amount and to surface characteristics (temperature and emissivity). The cloud signals that are investigated in the present study are significantly larger than the uncertainty caused by the calibration uncertainty (a few degrees K; e.g., Van de Berg *et al.* 1995). No absolute inter-calibration is performed. The resolution is degraded from 5 km to about 35 km in order to compare with the ECMWF model. This is done by re-mapping the native satellite images to an equal-angle latitude/longitude grid.

2.2 The model fields

The model version used in this study is the so-called cycle 23r3 of the ECMWF forecast system, which was operational in December 2000.

The assimilation system relies on the 4-dimensional variational scheme (4D-Var) described by Courtier *et al.* (1994). Analyses are produced at nominal times of 00 and 12 UTC, with an assimilation window of 12 hours. They use information about atmospheric pressure, temperature, water vapour and winds from conventional and satellite measurements. The clouds are not analysed, but the cloud fields from the 4D-Var final trajectory, therefore in balance with the analysed fields, are archived and used here. Most of the results presented here concern the 31 days of December 2000, with a time resolution of three hours. The times used and the corresponding forecast ranges are summarised in Table 1. Complementary computations, based on the analysis and on the 24-hour and 48-hour forecasts, are also performed but at 12 UTC only,

The forecast model is a global spectral $T_L511L60$ model. It includes a semi-Lagrangian advection scheme together with a linear Gaussian grid (Hortal 2000). The reduced horizontal grid corresponds to a regular grid size of about 40 km from the equator to the poles. In the

vertical, a hybrid coordinate of 60 levels between the surface and the top of the atmosphere is used by the global spectral forecast model. The physics package is based on Gregory *et al.* (2000). In particular, two prognostic equations describe the time evolution of cloud condensate and cloud cover (Tiedtke 1993), while rain and snow are separate diagnostic quantities. Clouds are formed by convection, diabatic cooling and boundary-layer turbulence. The scheme links their dissipation to adiabatic and diabatic heating, turbulent mixing of cloud air with unsaturated environmental air, and precipitation processes. The modifications to the original formulation from Tiedtke (1993) are given by Jakob and Klein (2000), Jakob (2000) and Jakob *et al.* (2000). The broad-band radiation scheme includes the Rapid Radiative Transfer Model (RRTM: Mlawer *et al.*, 1997) for the infrared and the Fouquart and Bonnel (1980) scheme (with four spectral bands) for the short-wave. At the surface, the Tiled ECMWF Scheme for Surface Exchanges over Land (TESSEL) described by Van den Hurk *et al.* (2000) is used.

The Meteosat infrared window (11 μm) radiances are simulated from the model profiles of temperature, specific humidity, cloud cover, ice water and liquid water, and from model surface variables (temperature and soil water). The method, that covers both infrared and micro-wave simulations, is described by Chevallier *et al.* (2001). It uses well-documented parameterisations that are summarised below. The gas absorption is obtained from the Radiative Transfer for Tiros Operational Vertical Sounder (RTTOV: Eyre 1991; Saunders *et al.* 1999). The radiances in the presence of semi-transparent cloud layers are expressed as a linear combination of the clear sky radiance and of the radiances in the presence of single layered black bodies (Washington and Williamson 1977). The coefficients of the linear combination are functions of the cloud cover and of the cloud emissivity on model levels. The cloud absorption is computed consistently with the ECMWF version of RRTM, with cloud absorption from Ebert and Curry (1992) for ice water and from Smith and Shi (1992) for liquid water. The maximum-random hypothesis defined by Räisänen (1998) is used to describe the overlap of the cloud layers. Scattering is not considered, which could lead to a slight overestimation of the brightness temperatures by the model, primarily for high thin clouds. Even though the satellite viewing angle is taken into account, the computed brightness temperatures may be overestimated for large zenith angles due to the neighbouring pixel clouds that are not taken into account (Joyce *et al.* 2001). Moreover, the maximum-random hypothesis is also less reliable for large angles. In order to limit these effects, the image pixels for which the satellite zenith angle is more than 70° are discarded, except in Figures 8 and 9. The estimation of surface emissivity differs from the ECMWF version of RRTM (Gregory *et al.* 2000). Emissivity is set to 0.99 and 0.93 respectively on moist and dry lands. The Infrared Surface Emissivity Model for RTTOV-6 (ISEM-6; Sherlock 1999) provides the sea emissivity.

2.3 Method of comparison

In the following, Meteosat images are compared to simulated images from the analyses and forecasts. All image manipulations are performed with the Man computer Interactive Data Access System (McIDAS) software (Lazzara *et al.* 1999). Statistics are computed in terms of mean, standard deviation and correlation. The correlation between two series of N numbers $\{a(i)\}_{i=1,N}$ and $\{b(i)\}_{i=1,N}$ (here brightness temperatures), with means $\bar{a}$ and $\bar{b}$, and standard deviations σ_a and σ_b, are given by:

$$cor(a,b) = \frac{1}{N} \sum_i \frac{(a(i) - \bar{a})(b(i) - \bar{b})}{\sigma_a \sigma_b} \qquad (1)$$

Two types of correlations are used: the series are either temporal (with i being the time index, with fixed spatial location) or spatial (with i being the space index, with fixed time).

The study focuses on cloud signals as seen from the infrared window channel. However the $11\mu m$ radiances are also sensitive to other quantities, mainly surface temperature, surface emissivity and water vapour continuum absorption. The uncertainty of the surface temperature in the model is of the order of a degree over sea and is larger over land. In particular its diurnal cycle is not taken into account over sea, and may be underestimated over land (Morcrette 2001). The surface emissivity depends on the surface characteristics, like skin temperature, soil water content, vegetation coverage and soil nature. Due to the uncertainty of those quantities, only a rough estimation of the emissivity is used here over land (section 2.2). As far as the water vapour is concerned, radiative computations show that it impacts the $11\mu m$ brightness temperature by about 3 K (respectively 9 K) when the total column water vapour is about 30 kg/m^2 (respectively 60 kg/m^2). The difficult representation of the humidity fields may affect the reproduction of this signal by the model computation. If the various errors accumulate, errors in the computation of the clear-sky brightness temperatures may reach 10 K or more over land. This non-negligible uncertainty is important to keep in mind when analysing the forthcoming results. As a consequence, effort is made here to link the patterns of the differences with the atmosphere dynamics, in order to identify them. A parallel study at ECMWF concerns the clear-sky differences but is out of the scope of the present one.

3 Results

3.1 December 2000 main general circulation patterns

Figure 1 illustrates the structure of the atmospheric flow during December 2000. It represents the mean 300 hPa horizontal wind field (Figure 1a) and that one on 15 December at 12 UTC (Figure 1b), analysed by the ECMWF system. The northern Atlantic jet stream is oriented towards Spain. In Europe it snakes north of the Mediterranean sea, then southward along the Arabic peninsula, before strengthening in south-east Asia. The sub-tropical jet streams wave around 20°N in the northern hemisphere and around 40°S in the southern hemisphere. The satellite images (e.g., Figure 2c and 2d) indicate that the Inter-Tropical Convergence Zone (ITCZ) is located at the Equator with a large southward extension over land.

3.2 Spatial variability

The mean values of the 11 μm brightness temperature for the month of December are presented in Figure 2. By comparison, the mean model surface temperature in the Meteosat-7 area is shown on Figure 3a. In the overlap region, the brightness temperatures from the two satellites differ by a few degrees K or less for instantaneous observations, because of differences in spectral response, calibration and viewing angle. The general patterns of the Meteosat images are well reproduced by the ECMWF system: the ITCZ over sea as over land, the trade wind regions, the land-based convergence zones, and the mid-latitude cyclone tracks. The intensity of the model patterns does not fit the observations so well, in particular over tropical lands (Brazil, southern Africa, Ceylon and Indonesia) where the ITCZ is strongly underestimated, with model

	Model fields	AN	FC12	FC24	FC48
Sea	Mean	0.765	0.745	0.724	0.682
	Standard deviation	0.025	0.025	0.028	0.035
Land	Mean	0.752	0.728	0.712	0.681
	Standard deviation	0.054	0.059	0.062	0.061

Table 2: Meteosat-7, 12 UTC. Mean and standard deviations of the time series of the spatial correlations between the simulated images and the observations from 12 October to 31 December 2000. Distinction is made between land and sea geotypes. The simulations use the analysis, the 12-hour, the 24-hour or the 48-hour forecasts (respectively AN, FC12, FC24 and FC48).

brightness temperatures warmer than the observations by more than 12 K. Conversely, over tropical oceans, the ITCZ intensity is overestimated by about 8 K or more. West of Senegal, the differences are about 10 K, the model being warmer than the observations. In the mid-latitude regions, the model is about 5 K warmer than the observations with larger differences over Europe: about 10 K. The agreement of the bias patterns with the cloud patterns, as well as its amplitude, suggests that it is caused by deficiencies of the cloud radiative forcing in the model. The cloud radiative forcing is defined as the difference between the clear-sky brightness temperature and the full-sky brightness temperature.

Focusing on Meteosat-7, Table 2 presents some statistics (mean and standard deviations) about the temporal evolution of the spatial correlation between the observed and the simulated images at 12 UTC over an extended period of time: from 12 October to 31 December 2000. The correlations for the analyses vary between 0.7 and 0.8 over ocean, with a mean of 0.765 and a standard deviation of 0.025. Over land, the variations are stronger, between 0.6 and 0.9 with a standard deviation of 0.054, depending on the spatial structure of the cloudiness. All latitudes are taken into account in these statistics. They are mostly representative of mid-latitude regions (poleward of 20°N and 20°S). When restriction is made to the 20°N-20°S band, correlations are poor: about 0.55 over sea as over land (not shown).

For the forecasts, Table 2 shows that the longer the range is, the lower the correlation is. Over sea, the 12-hour forecast mean correlation is 0.02 lower than the mean correlation using the analyses. The 24-hour forecast mean correlation is 0.02 further down, which is still a limited degradation in the forecast quality on an average. When reaching the 48-hour range the mean correlation goes down to 0.68. The good quality of the forecasts up to a 24-hour range is confirmed by direct examination of the images from both satellites (not shown). Over land, the degradation compared to the analysis correlation is stronger than over sea for the 12- and 24-hour. Also the standard deviations are about twice as high, which makes the forecasts less reliable over land. Focusing on December 2000, the correlations using the 3-, 6- and 9- hours forecasts (see Table 1) consistently vary between the analysis and the 12-hour correlations (not shown).

The Meteosat images allow validation of the scales of the spatial structures that the model describes. For each pixel of the Meteosat image (either simulated or observed), the nearest pixel that is correlated in time by less than 0.9 to that pixel is found. Figure 4 shows the distance to that nearest pixel for December 2000. In the following, the word “pixel” relates to the

reduced-resolution (35 km) images (see section 2.2). Over most regions, the observed images have distances of less than 40 km, which means that from one pixel to the next, the variability is usually more than 10%. In the mid-latitudes, in the northern hemisphere sub-tropical jet-stream and in the land-based convergence zones, the distance is about 50 km. Higher values are seen in the desert areas. In the model-simulated images, the distances are about 90 km (i.e. about three pixels), with lower values (about 60 km) in the trade winds and southern Africa, and higher values (more than 140 km) in the desert areas. This result confirms that the effective resolution of a model is lower than its numerical resolution (Pielke 1991, Laprise 1992).

3.3 Temporal variability

The brightness temperature standard deviations are presented in Figure 5. By comparison, the standard deviation of the model surface temperature in the Meteosat-7 area is shown on Figure 3b: they are usually less than 4 K. The brightness temperature standard deviations are much higher in most regions. They are lower in the model than in the observations by about 4 K over most areas, confirming the lack of representation of atmospheric variability illustrated in the previous section. Larger negative differences are found over the land parts of the ITCZ, where the standard deviations of the model are about 10 K lower than those of the observations, west of Senegal, with negative differences up to minus 15 K, and in the northern hemisphere mid-latitude disturbance regions, with negative differences about 7 K. This is consistent with the underestimation of the cloud forcing that is shown in Figure 2. Also, a model is expected to simulate an atmosphere smoother than the real one, because of the difficult representation of sub-grid processes.

Figure 6 shows the spatial variation of the temporal correlation between the model and the observations. Largest correlations (above 0.8) are found over the regions with less cloudiness, like the Sahara and Yemen, which seems to indicate a reasonable representation of the diurnal surface temperature cycle in these areas. Correlations above 0.7 are also located over mid-latitude lands and seas, in the border of the ITCZ, west of Senegal, east of Brazil, and over Namibia. The ITCZ, the trade wind regions, the high elevations in Asia, like the Himalayas and Mongolia, have low correlations. As an example of the model behaviour in the ITCZ over land, Figure 7 shows the brightness temperature mean and standard deviation as a function of the hour of the day in a 5° latitude by 5° longitude region over Zaire. Consistent with Figure 2, the model mean brightness temperature appears to be overestimated (between 10 and 20 K). Its diurnal cycle is less pronounced than in the observations, with a minimum during the afternoon and the night due to both surface temperature and cloudiness variations. The model standard deviation has a low diurnal variability, whereas the observations have a significant diurnal cycle that exhibits the afternoon maximum of convection. To summarise, the model locates the ITCZ well, but inadequately represents the time variations of convection, in particular over land.

4 Discussion

As in previous works (e.g., Morcrette 1991; Soden and Bretherton 1994; Roca *et al.* 1997; Chaboureau *et al.* 2000), the present study emphasises the use of geostationary satellites, like those of the Meteosat series, for the validation of numerical models of the atmosphere.

The high spatial and temporal resolution of these instruments allows extensive statistics to be gathered, so that models can be quantitatively monitored. For instance, it was shown that in the Meteosat data degraded to 35 km resolution, the variability of the brightness temperature time series usually differs by more than 10% from one grid point to another one, whereas the structures described by the model have scales of about three to four grid points at least (Figure 4). Also, forecast quality when going from a 3-hour range to a 24-hour range is very similar from the correlation point of view (Table 2). Unlike over sea, the spatial correlation over land is significantly degraded between the analysis and the forecasts. Moreover, the temporal variation of convection in the Tropics is not well represented, in particular over land (Figure 6). Improvements are needed in the modelling of the interaction between the soil, the planetary boundary layer and the atmosphere.

Some of the results presented confirm previous validation studies of the top-of-the-atmosphere radiation in earlier versions of the ECMWF model (Rizzi 1994; Chevallier and Morcrette 2000; Chevallier *et al.* 2001). These works rely on different instruments, different versions of the model and on different periods of time. In the extra-tropical cyclones, and to a lesser extent in the ITCZ, Chevallier *et al.* (2001) show that the model underestimates the radiative impact of high clouds, possibly because of insufficient cloud ice. As a result, the top-of-the-atmosphere long-wave radiation is overestimated in the frontal regions and in the ITCZ (Figure 2). In the oceanic ITCZ, the excessive frequency of cloud occurrence over time counter-balances this effect and leads to an underestimation of the top-of-the-atmosphere long-wave radiation, when averaged over long periods of time, as is done here. The overestimation of the radiation west of Senegal, despite good temporal correlations, is a feature that was not noted before. The Atlantic and African ITCZs provide moisture for the generation of cirrus clouds. This cirrus outflow is insufficiently represented in the model. The mis-representation of cirrus clouds in this region is confirmed by independent validation using the CO_2-slicing technique (Wylie *et al.* 1994) to retrieve cloud-top pressure from the High-resolution Infrared Radiation Sounder (HIRS) observations and from the model (not shown). The underestimation of the cloud forcing by the model partly explains the underestimation of the temporal variability of the top-of-the-atmosphere radiation (Figure 5). Pole-ward of 30°S and 30°N, the relatively high correlations in Figure 6 show that despite a weak cloud forcing in the model, the variations of the extra-tropical cyclones are well represented. This is illustrated on Figures 8 and 9 for 10 December: the model reproduces the location of the mid-latitude fronts very well (Figure 9), even over land. In comparison, the representation of the ITCZ is poor, in particular over Kenya (Figure 8).

The extension of the validation of the top-of-the-atmosphere radiation in NWP models is a consequence of the higher level of skill required from them, when they have to satisfy an extended range of applications from analysis to forecasting and to climate studies. It is planned to use routinely the diagnostics shown here for the monitoring of the ECMWF system, in addition to the current diagnostics based on the clear radiances (Munro *et al.* 2000). They are expected to help improve the model parameterisations. They will be extended to the other meteorological geostationary satellites. Additional information about the model will be diagnosed as new instruments become available such as the Spinning Enhanced Visible InfraRed Imager (SEVIRI) instrument, on-board Meteosat Second Generation (MSG), that combines the advantages of an imager and those of an infrared sounder. Finally, on-going work aims at an objective feedback from the observed differences on the model through variational data assimilation of the cloud-affected radiances (Janisková 2001).

Acknowledgements

The authors would like to thank J.-J. Morcrette and C. Köpken for fruitful discussions about radiation in general and the Meteosat observations in particular. J.-J. Morcrette, A. Simmons, J.-N. Thépaut and three anonymous reviewers helped improve the initial version of the text.

References

Chaboureau, J.-P., J.-P. Cammas, P. Mascart, J.-P. Pinty, C. Claud, R. Roca, and J.-J. Morcrette, 2000: Evaluation of a cloud system life-cycle simulated by Meso-NH during FASTEX using METEOSAT radiances and TOVS-3I cloud retrievals. *Q. J. R. Meteorol. Soc.*, **126**, 1735-1750.

Chevallier, F., and J.-J. Morcrette, 2000: Comparison of model fluxes with surface and top-of-the-atmosphere observations. *Mon. Wea. Rev.*, **128**, 3839-3852.

Chevallier, F., P. Bauer, G. Kelly, C. Jakob, and T. McNally, 2001: Model clouds over oceans as seen from space: comparison with HIRS/2 and MSU radiances. *J. Climate*, in press.

Courtier, P., J.-N. Thépaut, and A. Hollingsworth, 1994: A strategy, for operational implementation of 4D-Var, using an incremental approach. *Q. J. Roy. Meteor. Soc.*, **120**, 1367-1388.

Ebert, E. E. and J. A. Curry, 1992 : A parameterization of cirrus cloud optical properties for climate models. *J. Geophys. Res.*, **97D**, 3831-3836.

Eyre, J. R., 1991: A fast radiative transfer model for satellite sounding systems. *ECMWF Technical Memorandum No. 176*, 28 pp.

Fouquart, Y. and B. Bonnel, 1980: Computation of solar heating of the Earth's atmosphere: a new parameterization. *Beitr. Phys. Atmosph.*, **53**, 35-62.

Gregory, D., J.-J. Morcrette, C. Jakob, A. C. M. Beljaars, and T. Stockdale, 2000: Revision of convection, radiation and cloud schemes in the ECMWF Integrated Forecasting System. *Q. J. Roy. Meteor. Soc.*, **126**, 1685-1710.

Hortal, M., 2000: The development and testing of a new two-time-level semi-Lagrangian scheme (SETTLS) in the ECMWF forecast model. *Q. J. Roy. Meteor. Soc.*, in press.

Jakob, C., 1999: Cloud cover in the ECMWF reanalysis. *J. Climate*, **12**, 947-959.

Jakob, C., 2000: The representation of cloud cover in atmospheric general circulation models.

PhD thesis, Ludwig-Maximilians-Universität München, 193 pp.

Jakob, C., and S. A. Klein, 2000: A parametrization of the effects of cloud and precipitation overlap for use in general-circulation models. *Q. J. Roy. Meteor. Soc.*, **126**, 2525-2544.

Jakob, C., E. Andersson, A. Beljaars, R. Buizza, M. Fisher, E. Gérard, A. Ghelli, P. Janssen, G. Kelly, A. P. McNally, M. Miller, A. Simmons, J. Teixeira, and P. Viterbo, 2000: The IFS cycle CY21r4 made operational in October 1999. *ECMWF Newsletter*, **87**, 2-9.

Janisková, M., 2001: Preparatory studies for the use of observations from the Earth radiation Mission in Numerical Weather Prediction. *Report from ESA contract No. 13151/98/NL/GD*, 79 pp. [available from ECMWF, Shinfield Park, Reading, Berks. RG2 9AX, UK].

Joyce, R., J. Janowiak, and G. Huffman, 2001: Latitudinally and seasonally dependent zenith-angle corrections for geostationary satellite IR brightness temperatures. *J. Appl. Meteor.*, **40**, 689-703.

Laprise, R., 1992: The resolution of global spectral models. *Bull. Amer. Meteor. Soc.*, **73**, 1453-1454.

Lazzara, M. A., J. Benson, R. Fox, D. Laitsch, J. Rueden, D. Santek, D. Wade, T. Whittaker, J. T. Young, 1999: The Man computer Interactive Data Access System (McIDAS): 25 Years of Interactive Processing. *Bull. Amer. Meteor. Soc.*, **80**, 271-284.

Mlawer, E. J., S. J. Taubman, P. D. Brown, M. J. Iacono, and S. A. Clough, 1997: Radiative transfer for inhomogeneous atmospheres : RRTM, a validated correlated-k model for the longwave. *J. Geophys. Res.*, **102**, 16663-16682.

Morcrette, J.-J., 1991: Evaluation of model-generated cloudiness: satellite observed and model-generated diurnal variability and brightness temperature. *Mon. Wea. Rev.*, **119**, 1205-1224.

Morcrette, J.-J., 2001: Assessment of the ECMWF model cloudiness and surface radiation fields at the ARM-SGP site. *ECMWF Technical Memorandum No. 327*, 41 pp. [available from ECMWF, Shinfield Park, Reading, Berks. RG2 9AX, UK].

Munro, R., G. Kelly, and R. Saunders, 2000: Assimilation of Meteosat Radiance Data within the 4DVAR System at ECMWF. EUMETSAT/ECMWF fellowship programme, Research report No. 8, 41 pp [available from ECMWF, Shinfield Park, Reading, Berks. RG2 9AX, UK].

Pielke, R. A, 1992: A recommended specific definition of "resolution". *Bull. Amer. Meteor. Soc.*, **72**, 1914.

Räisänen, P., 1998: Effective longwave cloud fraction and maximum-random overlap clouds - a problem and a solution. *Mon. Wea. Rev.*, **126**, 3336-3340.

Rizzi, R., 1994: Raw HIRS/2 radiances and model simulations in the presence of clouds. ECMWF Technical Memorandum No. 73, 29 pp. [available from ECMWF, Shinfield Park, Reading, Berks. RG2 9AX, UK].

Roca, R., L. Picon, M. Desbois, H. Le Treut, and J.-J. Morcrette, 1997: Direct comparison of Meteosat water vapor channel data and general circulation model results. *Geophys. Res. Letters*, **24**, 147-150.

Rohn, M., G. Kelly, and R. W. Saunders, 2001: Impact of New Cloud Motion Wind Product From Meteosat on NWP Analyses and Forecasts. *Mon. Wea. Rev.*, in press.

Rossow, W. B., and R. A. Schiffer, 1983: The International Satellite Cloud Climatology Project (ISCCP): the first project of the World Climate Research Program. *Bull. Amer. Meteo. Soc.*, **64**, 779-784.

Saunders, R., M. Matricardi, and P. Brunel, 1999: An improved fast radiative transfer model for assimilation of satellite radiance observations. *Quart. J. Roy. Meteor. Soc.*, **125**, 1407-1425.

Sherlock, V. J., 1999: ISEM-6: Infrared Surface Emissivity Model for RTTOV-6. The Met. Office, Forecasting Research Tech. Rep. FR-299, 17 pp. [available from The Met. Office, London Road, Bracknell RG12 2SZ, UK].

Schmetz, J., K. Holmlund, J. Hoffman, B. Strauss, B. Mason, V. Gaertner, A. Koch, L. Van De Berg 1993: Operational cloud-motion winds from Meteosat infrared images. *J. Appl. Met.*, **32**, 1206-1225.

Smith, E. A., and L. Shi, 1992: Surface forcing of the infrared cooling profile over the Tibetan plateau. Part I: Influence of relative longwave radiative heating at high altitude. *J. Atmos. Sci.*, **49**, 805-822.

Soden, B., and F. Bretherton, 1994: Upper-tropospheric relative humidity from the GOES 6.7μm channel - Method and climatology for July 1987. *J. Geophys. Res.*, **99**, 1187-1210.

Tiedtke, M., 1993: Representation of clouds in large-scale models. *Mon. Wea. rev.*, **121**, 3040-3061.

Van de Berg, L. C. J., J. Schmetz, and J. Whitlock, 1995: On the calibration of the Meteosat water vapor channel. *J. Geophys. Res.*, **100**, 21,069-21,076.

Van den Hurk, B. J. J. M., P. Viterbo, A. C. M. Beljaars, and A. K. Betts, 2000: Offline validation of the ERA40 surface scheme. ECMWF Technical Memorandum No. 295, 42 pp. [available from ECMWF, Shinfield Park, Reading, Berks. RG2 9AX, UK].

Velden, C. S., C. M. Hayden, W. P. Menzel, J. L. Franklin, and J. S. Lynch 1992: The impact of satellite-derived winds on numerical hurricane track forecasting. *Weather and Forecasting*, **7**, 107-118.

Velden, C. S., S. J. Niemann, W. P. Menzel, and S. T. Wanzong 1997: Upper tropospheric winds derived from geostationary satellite water vapour observations. *Bull. Amer. Meteor. Soc.*, **78**, 173-195.

Washington, W. M. and D. L. Williamson, 1977: A description of the NCAR GCM. In *Methods in Computational Physics*, **17** J. Chang. (Ed.), Academic Press, New York, 111-172.

Wylie, D. P., W. P. Menzel, H. M. Woolf, and K. I. Strabala, 1994: Four years of global cirrus cloud statistics using HIRS. *J. Climate*, **7**, 1972-1986.

Yu, W., L. Garand, and A. P. Dastoor, 1997: Evaluation of model clouds and radiation at 100 km scale using GOES data. *Tellus*, **49A**, 246-262.

(a)

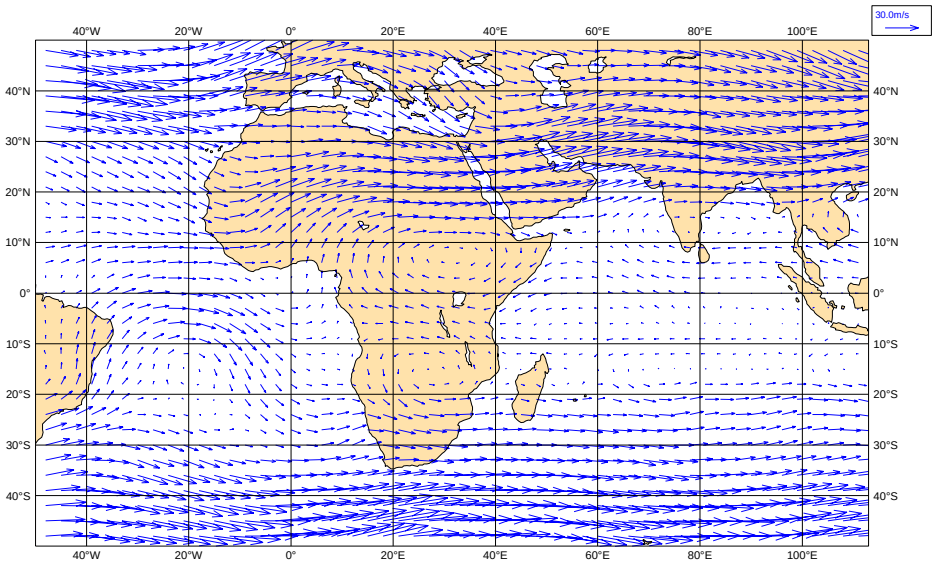

(b)

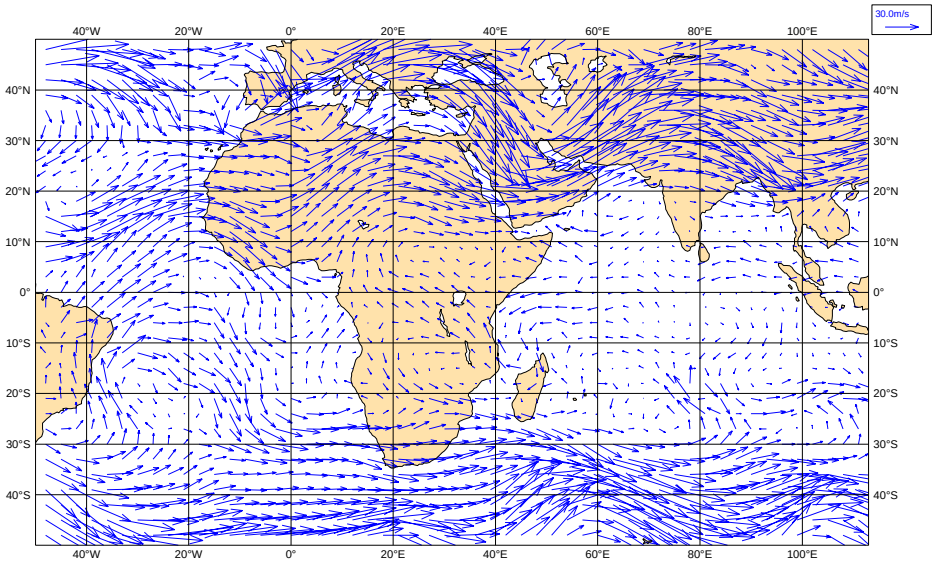

Figure 1: The horizontal wind field at 300 hPa from the ECMWF analyses: - (a) December 2000 monthly mean, - (b) on 15 December 2000, 12 UTC.

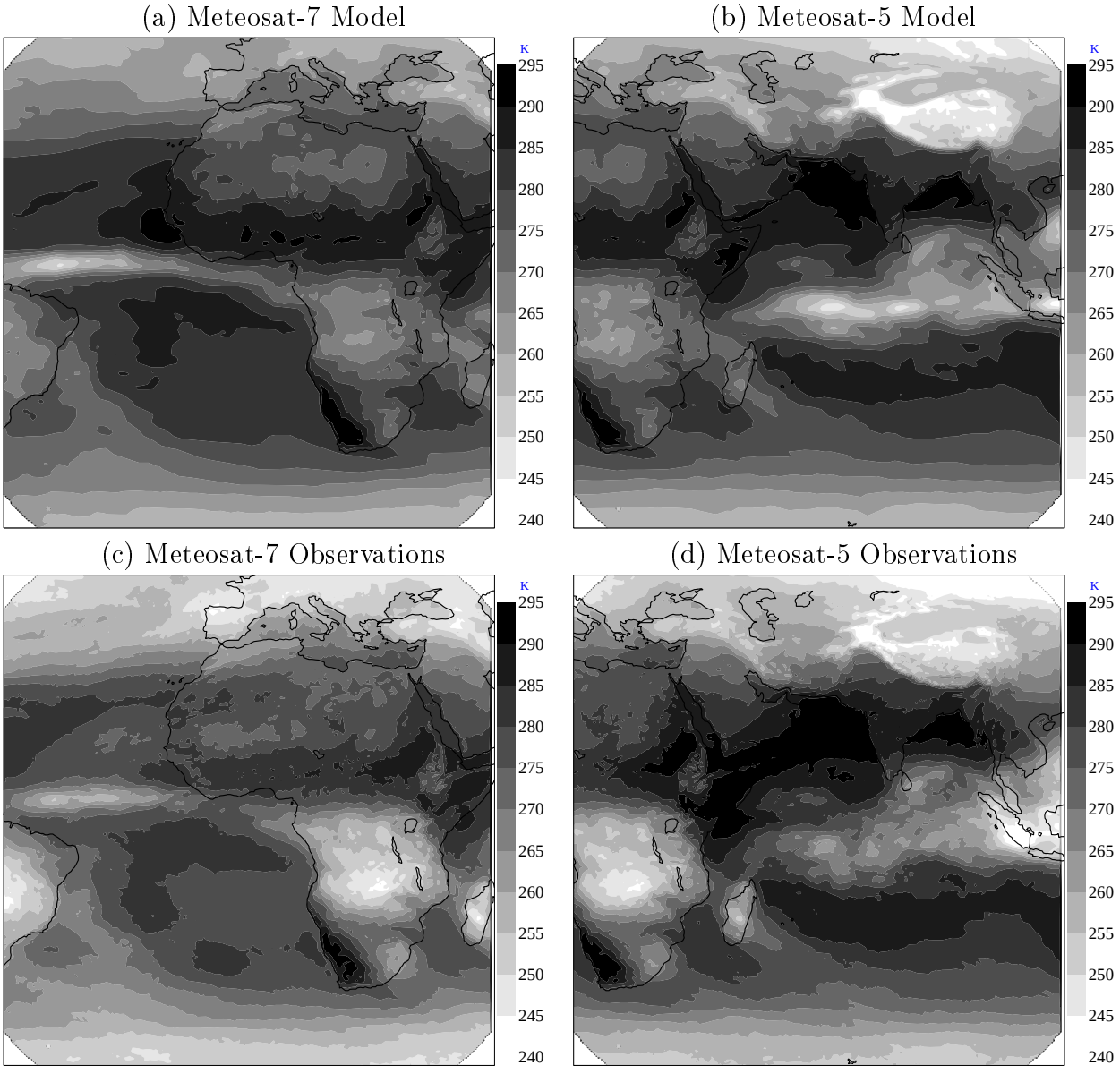

Figure 2: December 2000. Meteosat-7 and -5 mean $11\mu m$ brightness temperature.

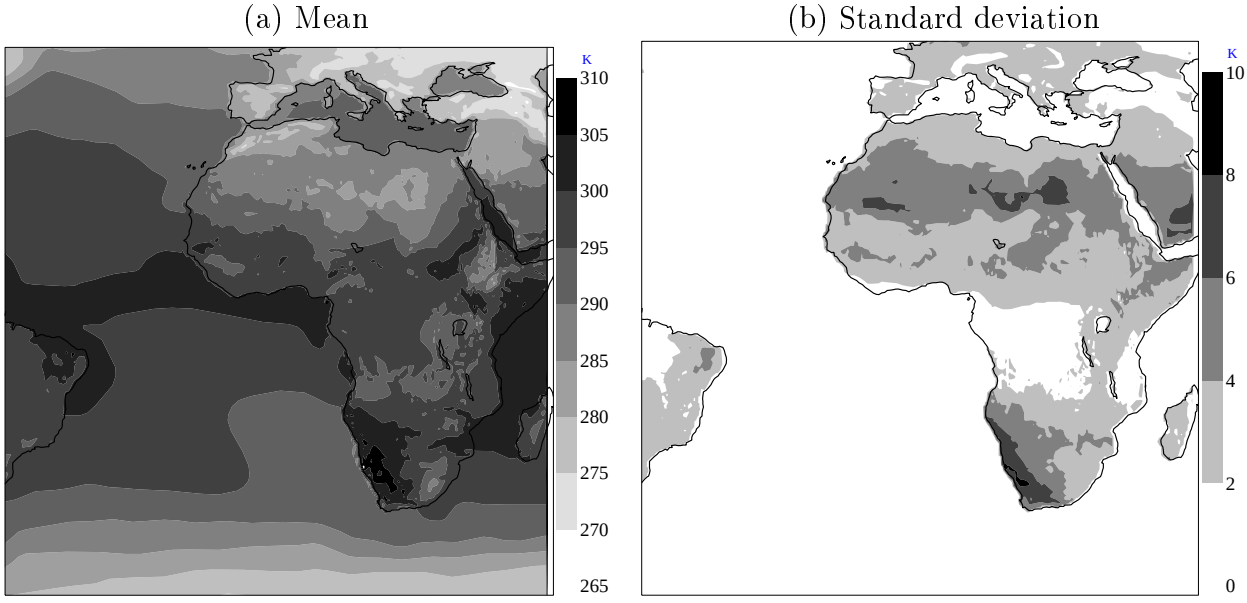

Figure 3: December 2000. Mean (a) and standard deviation (b) of the model surface temperature, in K, in the Meteosat-7 area.

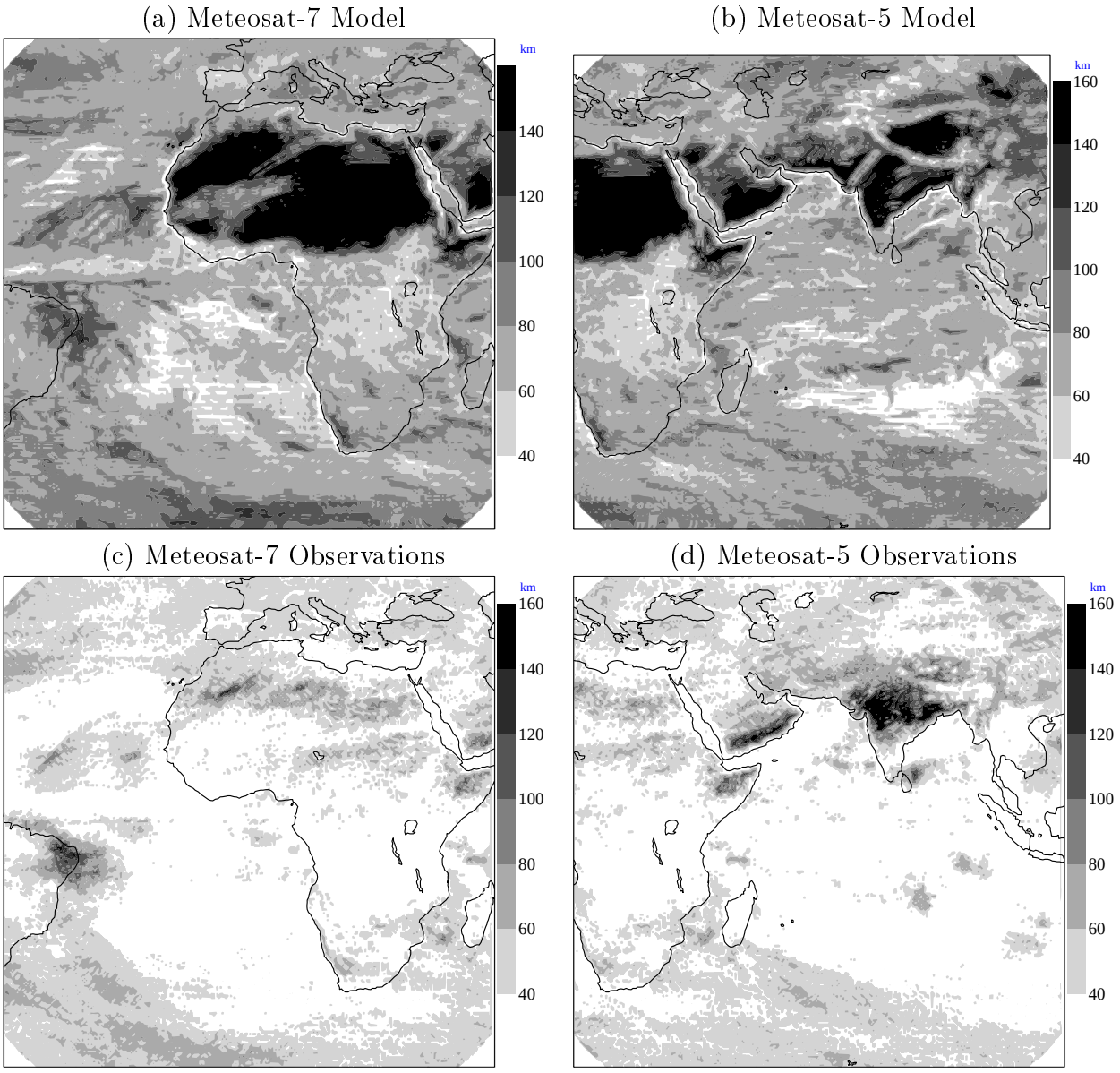

Figure 4: December 2000. For each pixel p of a Meteosat picture, the distance (in km) to the first pixel p' that is correlated in time by less than 0.90 to p, is represented.

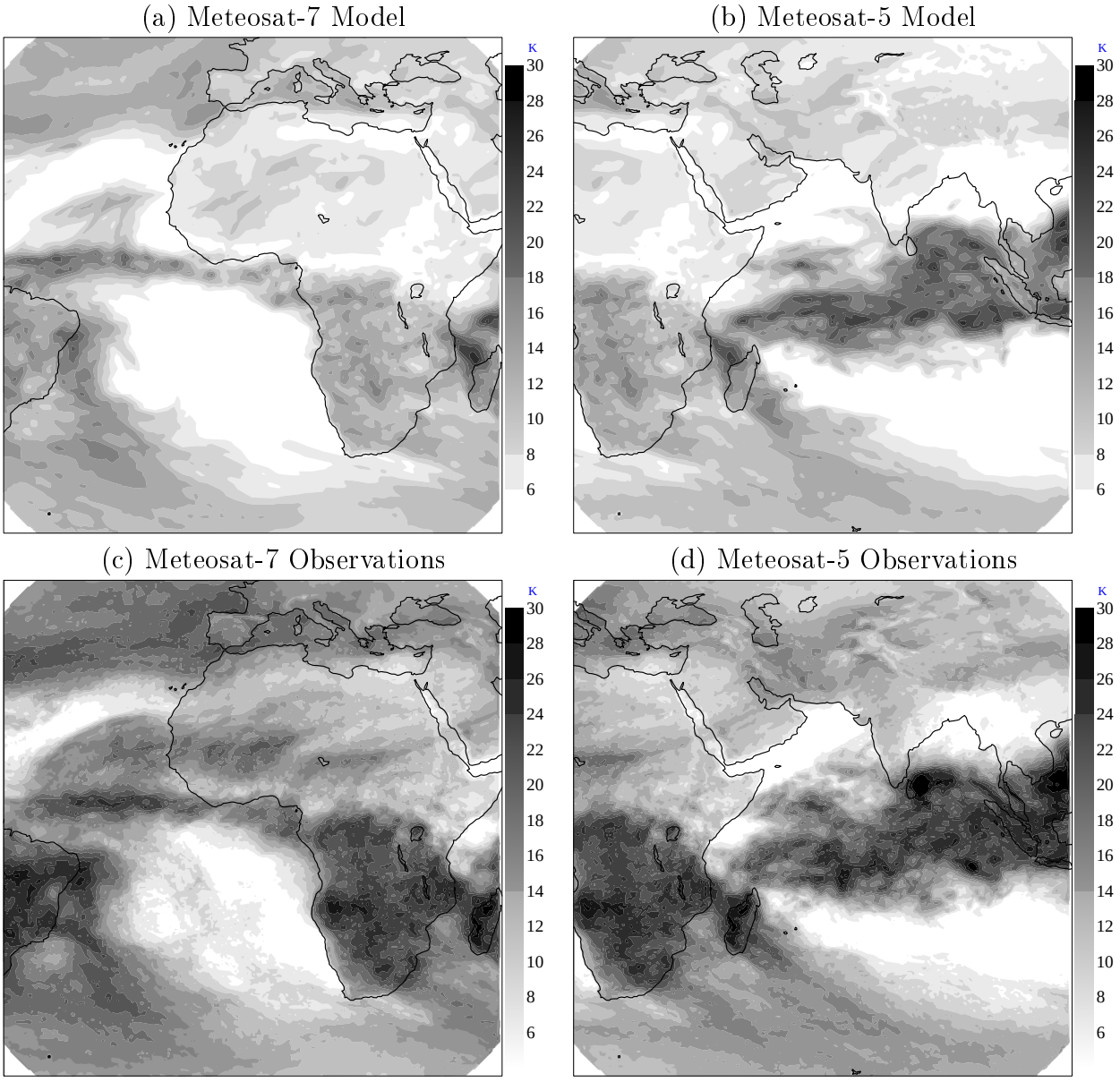

Figure 5: December 2000. Meteosat-7 and -5 standard deviation of the $11\mu m$ brightness temperature.

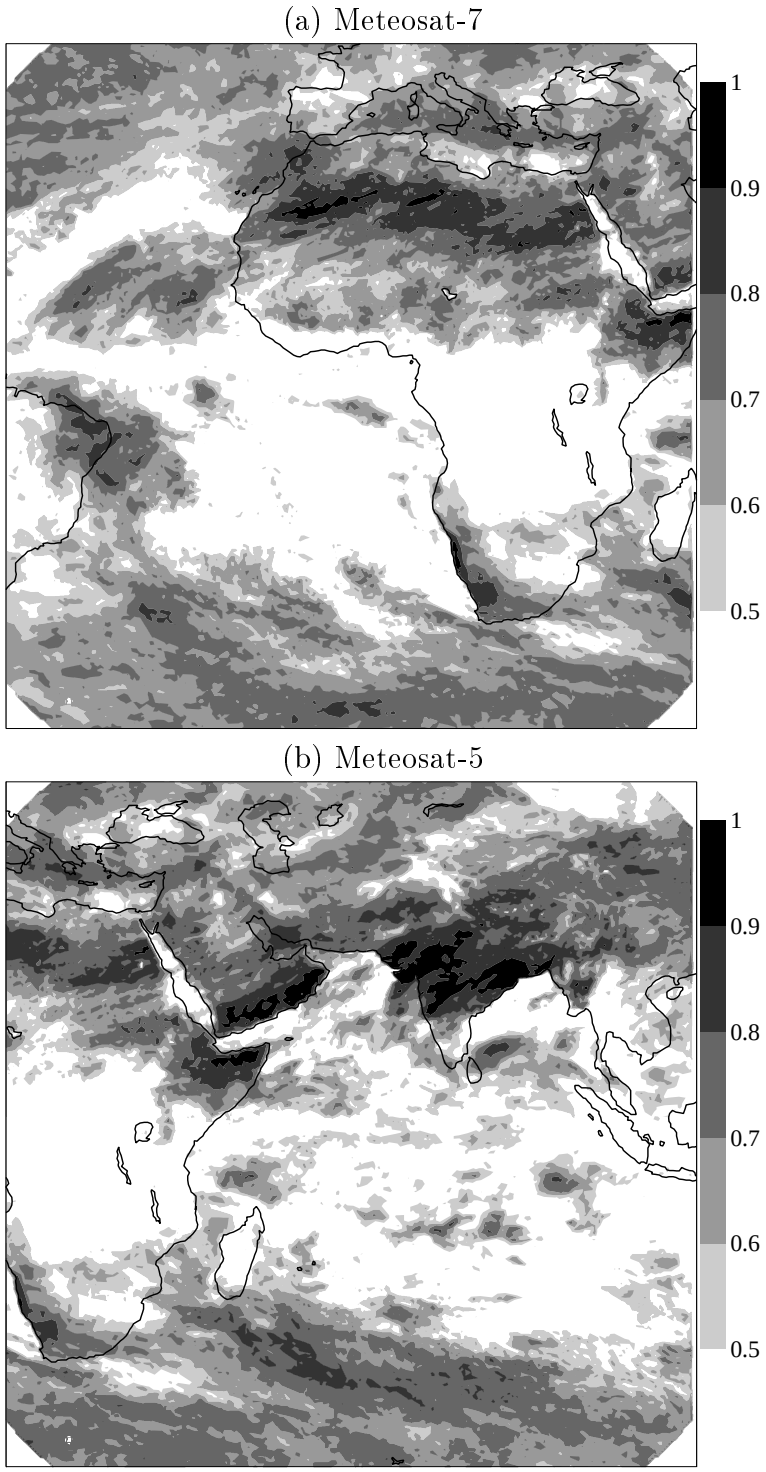

Figure 6: December 2000. Temporal correlation between the model-simulated and the observed $11\mu m$ brightness temperatures.

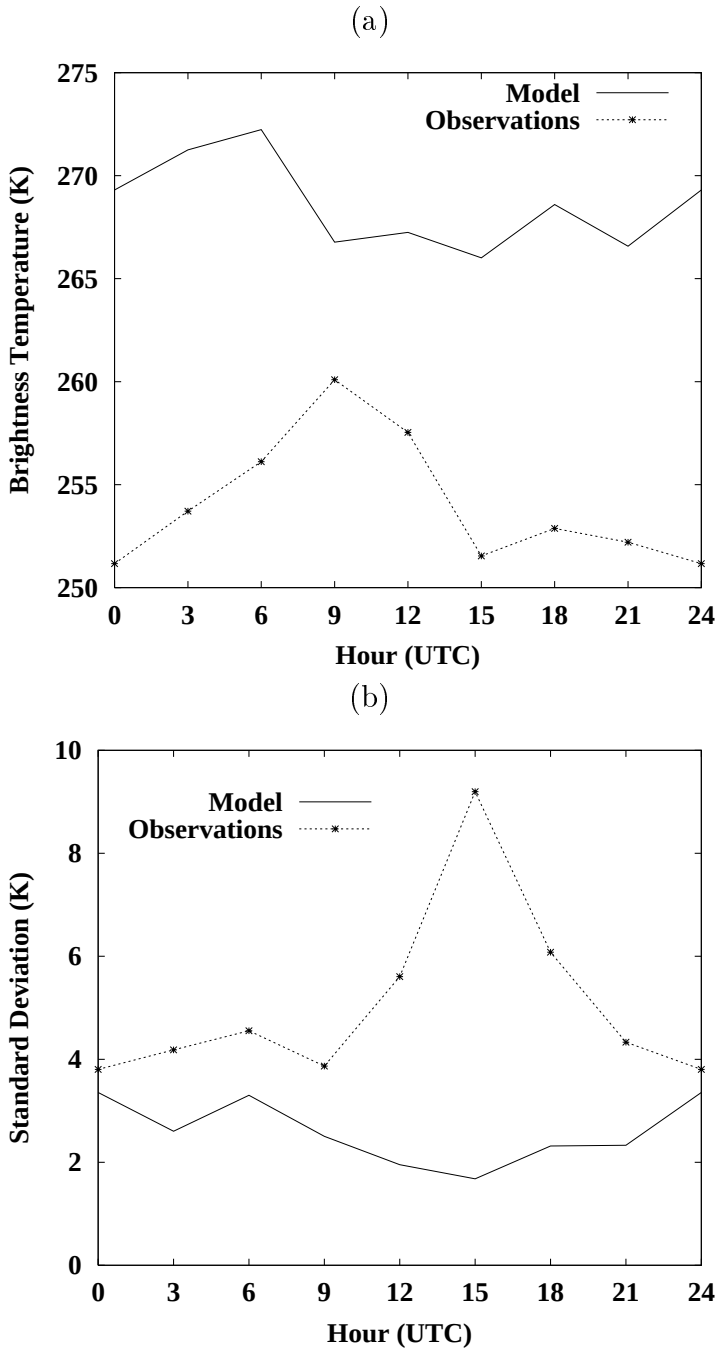

Figure 7: December 2000. Brightness temperature mean (a) and standard deviation (b) as a function of the hour of the day in the 20°E-25°E and 5°S-Equator region (Zaire).

(a) Model

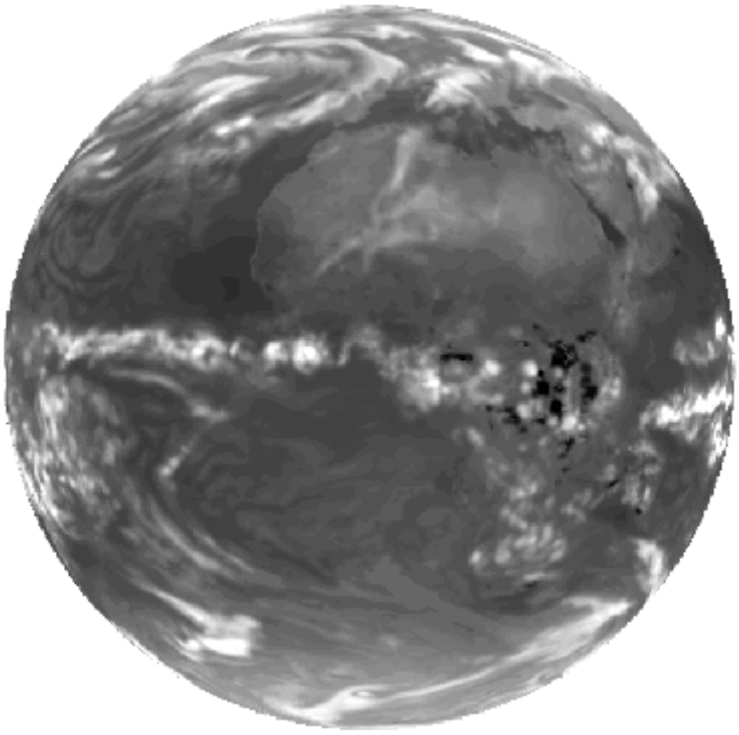

(b) Observation

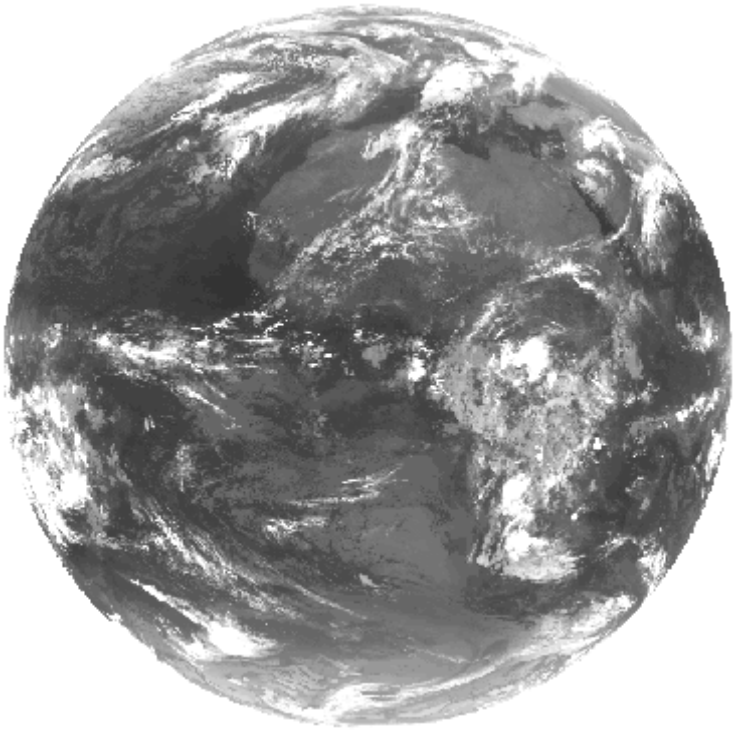

Figure 8: 10 December 2000, 03 UTC. Simulated and observed Meteosat 11μm image. The simulation was performed on the 3-hour forecast. The grey scale is the same in (a) and (b).

(a) Model

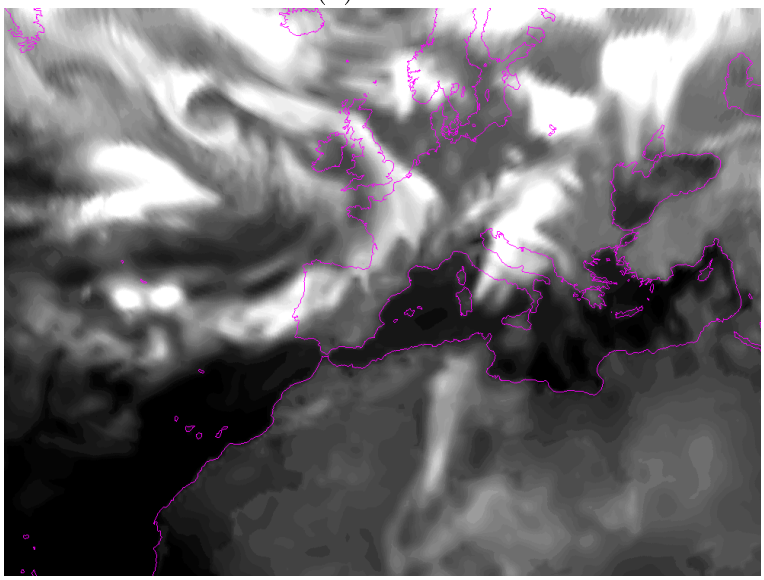

(b) Observation

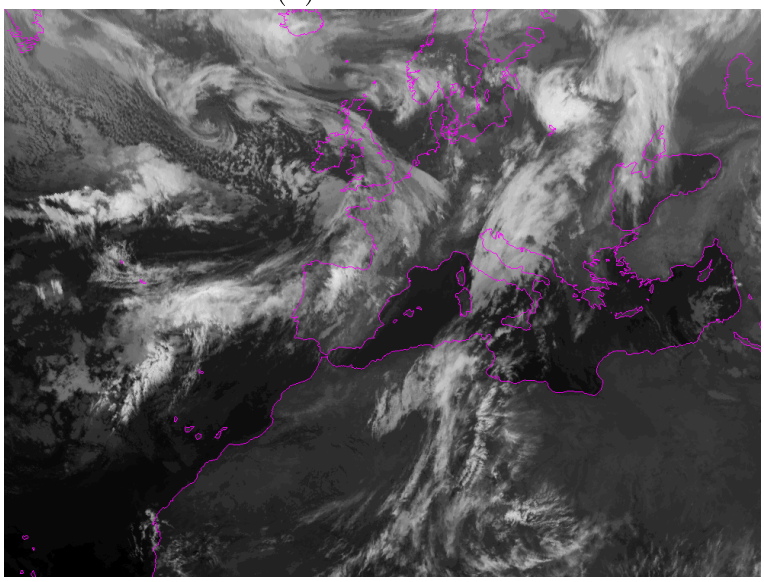

Figure 9: 10 December 2000, 03 UTC. Simulated and observed Meteosat 11μm image. The simulation was performed on the 3-hour forecast. In order to highlight the cloud patterns, the grey scale differs between (a) and (b).